CrystEngComm

COMMUNICATION

View Article Online
View Journal | View Issue

Cite this: *CrystEngComm*, 2025, **27**, 3433

Received 3rd April 2025,
Accepted 23rd April 2025

DOI: 10.1039/d5ce00366k

rsc.li/crystengcomm

Concentration- and temperature-dependent variation of Co_3O_4 nanoparticle size and morphology: insights into the growth behaviour and scalability†

Johannes Kießling*[a] and Anna S. Schenk *[ab]

Colloidally stable Co_3O_4 nanoparticles with diameters of 5–16 nm and a concentration-dependent transition from cuboidal to cubic morphologies are synthesised in ambient atmosphere. Through systematic variation of reagent concentration, temperature, and growth time, controllable adjustments of the particle size along with narrow size distributions as low as 12% are achieved. The scalability of the synthesis and the remarkable stability during the growth regime ensure sufficient yield for technical applications.

Materials with nanoscale dimensions play an important role in various technological fields as they allow the manipulation of physical properties through down-scaling the size of their structural motifs.[1–3] These size effects, render the study of nanomaterials a compelling field of research.[4,5] Co_3O_4 nanoparticles (NPs), in particular, exhibit diverse applications, including catalysis, energy storage, and sensors.[6–8] When used as a catalyst, Co_3O_4 NPs are applied for industrial processes such as the Fischer–Tropsch synthesis and water-splitting for clean energy generation.[9–11] Due to the relatively high earth abundance, Co is more cost-effective than other efficient transition metal catalysts (*i.e.* Pd, Ir, Pt) while still providing desirable catalytic efficiency.[12–14] As NPs possess a high surface area, they are greatly suitable for surface-dependent reactions. The development of facile, high-yield synthesis strategies providing control over particle size and shape at narrow size distributions is crucial for any prospect in application.

We recently reported a facile and inexpensive synthetic route towards colloidally stable Co_3O_4 NPs with tuneable size.[15] In this co-precipitation approach, cobalt hydroxide precursor particles are initially formed and subsequently thermally converted *in situ* into Co_3O_4. In order to further control NP size and shape and to achieve tailored size- and morphology-dependent properties, however, an in-depth understanding of nucleation and growth during the crystallization process is required.[16,17] Therefore, we here expand on the previous promising results by systematically investigating the effects of concentration and temperature on the crystallization of Co_3O_4 NPs. Most importantly, the influence of the growth time is examined for several concentrations and particle development is monitored by aliquot extraction followed by transmission electron microscopy (TEM) image analysis. We further demonstrate the scalability of the synthesis.

Size control through systematic variation of reaction temperature and reagent concentration

The general synthetic strategy used for the herein presented growth studies has been introduced in detail in our previous work.[15] Briefly, $Co(NO_3)_2{\cdot}6H_2O$ is dissolved in oleylamine (OLA), which acts as solvent and stabilizing ligand, mixed with a small amount of EtOH as a phase mediator. Cobalt hydroxide precursor particles are precipitated from these Co(II) solutions with a stoichiometric amount of NaOH (aq) and subsequently converted to Co_3O_4 by raising the temperature to at 180 °C. To systematically examine the effects of variable reaction parameters, Co_3O_4 NPs were here synthesized at different temperatures (T = 60–100 °C) and reagent concentrations ([$Co(NO_3)_2{\cdot}6H_2O$] = 0.1–0.4 M). The used amounts of substance are 2, 4, 6, and 8 mmol of $Co(NO_3)_2{\cdot}6H_2O$ in 20 mL OLA to implement nominal concentrations of 0.1, 0.2, 0.3, and 0.4 mol L^{-1}. For brevity, samples are coded according to the following scheme: $\text{Temperature}^{\text{growth time}}_{\text{mass of substance}}$.

An exemplary series of particles synthesized at T = 90 °C with variable reagent concentrations is displayed in Fig. 1

[a] *Physical Chemistry IV, University of Bayreuth, Universitaetsstrasse 30, 95447 Bayreuth, Germany. E-mail: johannes.kiessling@uni-bayreuth.de, anna.schenk@uni-bayreuth.de*

[b] *Bavarian Polymer Institute (BPI), University of Bayreuth, Universitaetsstrasse 30, 95447 Bayreuth, Germany*

† Electronic supplementary information (ESI) available: Detailed synthesis protocols, X-ray and electron diffractograms, TEM micrographs of nanoparticle samples extracted at different growth stages, particle size histograms, summary of average particle sizes and size distributions, discussion of concentration-dependent morphological modulations. See DOI: https://doi.org/10.1039/d5ce00366k

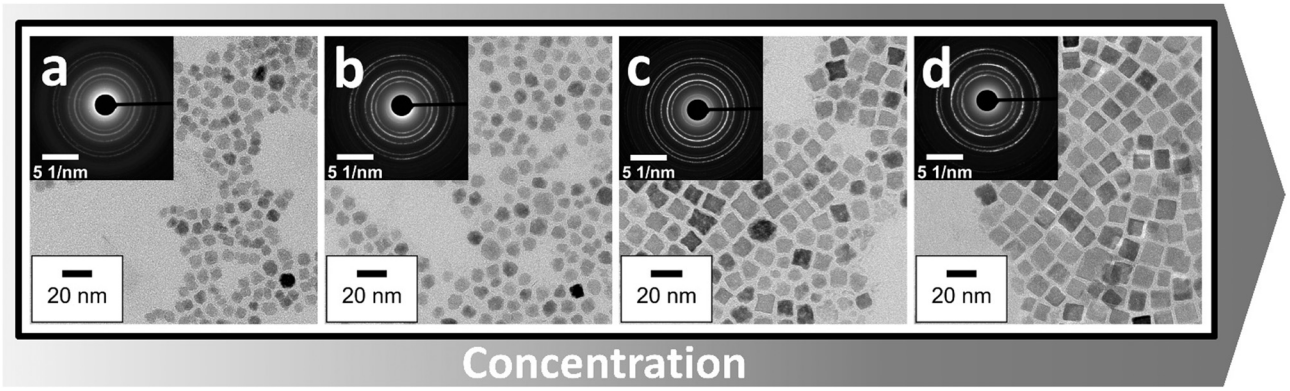

Fig. 1 TEM micrographs of Co_3O_4 nanoparticles synthesized at T = 90 °C with a growth time of 1 h and increasing amounts of the reagent $Co(NO_3)_2{\cdot}6H_2O$ in 20 mL OLA: a) $n(Co(NO_3)_2{\cdot}6H_2O)$ = 2 mmol, b) $n(Co(NO_3)_2{\cdot}6H_2O)$ = 4 mmol, c) $n(Co(NO_3)_2{\cdot}6H_2O)$ = 6 mmol, and d) $n(Co(NO_3)_2{\cdot}6H_2O)$ = 8 mmol. Insets: corresponding selected area electron diffraction patterns.

showing increasing size and regularity. X-ray diffraction analysis and selected area electron diffraction (SAED) confirm that phase-pure Co_3O_4 is formed as the product phase after thermal conversion at 180 °C (*cf.* Fig. 1 and S1–S3† for detailed graphs and analyses). The temperature- and concentration-dependent particle sizes and particle size distributions (PSD) are summarized in Table 1 and the full set of corresponding TEM micrographs is presented in the ESI† (SI; *cf.* Fig. S4). The PSD may be regarded as a quality criterion for the chosen synthetic conditions, as narrower NP size distributions are usually associated with more uniform physicochemical properties.[18]

At T = 100 °C, using an elevated reagent amount of 10 mmol $Co(NO_3)_2{\cdot}6H_2O$ results in a conspicuously broad PSD (*i.e.* >25%). This observation suggests insufficient solubility of the $Co(NO_3)_2{\cdot}6H_2O$ salt in OLA to support higher concentrations than the here considered range of 2–8 mmol in 20 mL OLA (*cf.* Fig. S5†). Similarly broad PSDs pertain to experiments of type 60^{1h}_{4mmol}, 60^{1h}_{6mmol}, and 70^{1h}_{8mmol}. The literature-reported decomposition temperature of solid $Co(NO_3)_2{\cdot}6H_2O$ is 100 °C, thus coinciding with the onset of water boiling.[19] However, it is possible to synthesize Co_3O_4 NPs at elevated temperatures above 100 °C (*cf.* Fig. S6†), as the decomposition of $Co(NO_3)_2{\cdot}6H_2O$ dissolved in OLA proceeds only at T >125 °C. Notably, at T = 100 °C, Co_3O_4 NPs may even be synthesized in the absence of NaOH as a precipitation agent, yet with a broad bi-modal PSD (*cf.* Fig. S7†).

Individual experiments (Table 1) systematically investigate the impact of the Co(II) salt concentration at temperatures between 60–100 °C, varying the parameters independently. Overall, the size decreases with increasing temperature.[15] In the temperature range between 70–90 °C, enhancing the amount of $Co(NO_3)_2{\cdot}6H_2O$ from 2 mmol to 4 mmol does not significantly alter the particle size. In general, the size increases with the monomer concentration with an outlier for sample 70^{1h}_{8mmol}, where the concentration possibly exceeds the system's solubility limit. In terms of the PSD noticeable differences in solubility become apparent. At T = 100 °C, the PSD systematically decreases with the concentration. Similar trends are observed at lower temperatures, even though the differences in PSD are less pronounced in these cases. This leads to occasional data outliers where higher concentrations lead to a slightly broader PSD. Among those, sample 80^{1h}_{8mmol} may be close to the solubility limit of the system at T = 80 °C, contributing to an increase in PSD. In comparison, the PSD is almost 10% narrower for sample 90^{1h}_{8mmol}. While experiments at T = 60 °C are included for completeness, their applicability appears limited. Solely sample 60^{1h}_{2mmol} achieves an acceptable PSD which, however, increases considerably at higher salt concentrations.

Morphologically, the particles tend to appear quasi-spherical or cuboidal at lower concentrations (2–4 mmol). The same phenomenon also applies to higher concentrations (6–8 mmol) at moderate temperatures of T = 70–80 °C. When the reaction temperature is increased to T = 90–100 °C, however, the particle morphology shifts to cubic for $n(Co(NO_3)_2{\cdot}6H_2O)$ = 6–8 mmol. The changes in size and morphology are readily apparent at T = 90 °C where the largest particles (90^{1h}_{8mmol}) of this work were achieved (Fig. 1).

Table 1 Average particle diameters [nm] and particle size distribution (PSD, absolute and percentage) of Co_4O_4 NPs obtained at different synthetic parameters under systematic variation of temperature and $Co(NO_3)_2{\cdot}6H_2O$ concentration [mmol]. The volumes of the solvent (OLA) and co-solvents (EtOH, H_2O) are kept constant

T [°C]	2 mmol [nm]	4 mmol [nm]	6 mmol [nm]	8 mmol [nm]
60	5.38 ± 1.10 20.4%	8.60 ± 2.88 33%	8.10 ± 2.18 27%	—
70	13.67 ± 2.52 18.4%	13.65 ± 3.01 22.0%	15.40 ± 2.88 18.7%	13.75 ± 4.10 29.8%
80	12.52 ± 3.10 24.7%	13.04 ± 2.10 16.1%	14.61 ± 2.87 19.7%	15.22 ± 3.66 24.0%
90	10.81 ± 2.03 18.5%	10.77 ± 1.55 14.4%	14.85 ± 2.93 19.7%	15.66 ± 2.27 14.5%
100	8.65 ± 2.04 23.6%	10.20 ± 1.82 17.8%	10.61 ± 1.62 15.2%	13.49 ± 1.63 12.04%

Up-scaling of the Co_3O_4 nanoparticle synthesis

To enhance the particle yield, up-scaling of the educt and solvent amounts used in an experiment is an intuitive and appealing option (see ESI†). In general, the yield increases with the reagent concentration in the presented precipitation system. On a laboratory scale, a fivefold up-scaling of the 100^{1h}_{8mmol} experiment yielded >1 g of purified nanoparticles, thus highlighting the scalability of the synthetic approach towards quantities relevant in technical settings, where Co_3O_4 NPs find a plethora of applications, *e.g.* in electrocatalysis.

Co_3O_4 nanoparticle growth-series experiments

Scientifically, up-scaling of the presented synthesis to larger volumes is additionally beneficial for monitoring the growth of NPs by TEM analysis through aliquot extraction. This approach allows for the construction of growth curves, providing insights into the development of the precipitation system at different stages of particle formation. For time-dependent studies of the NP size evolution, a total of 19 aliquots (á 200 μL) of NP dispersion were withdrawn from the reaction with a sterile syringe at dedicated reaction times between 1–240 min (*cf.* Fig. S8–S11†).

The measured NP sizes are summarized in Tables S4–S7.† The total volume of 19 aliquots amounts to 3.8 mL. For a reaction with 20 mL of OLA, this represents *ca.* 19% of the full volume. Even in this case, no obvious negative effects of the extraction process on the particle growth were observed (based on a comparison of the final products with particles obtained in analogous reactions performed at constant volume). However, for recording the presented growth curves (Fig. 2), an up-scaled reaction mixture with 60 mL OLA was used, with aliquots amounting to *ca.* 6.3% of the full volume,

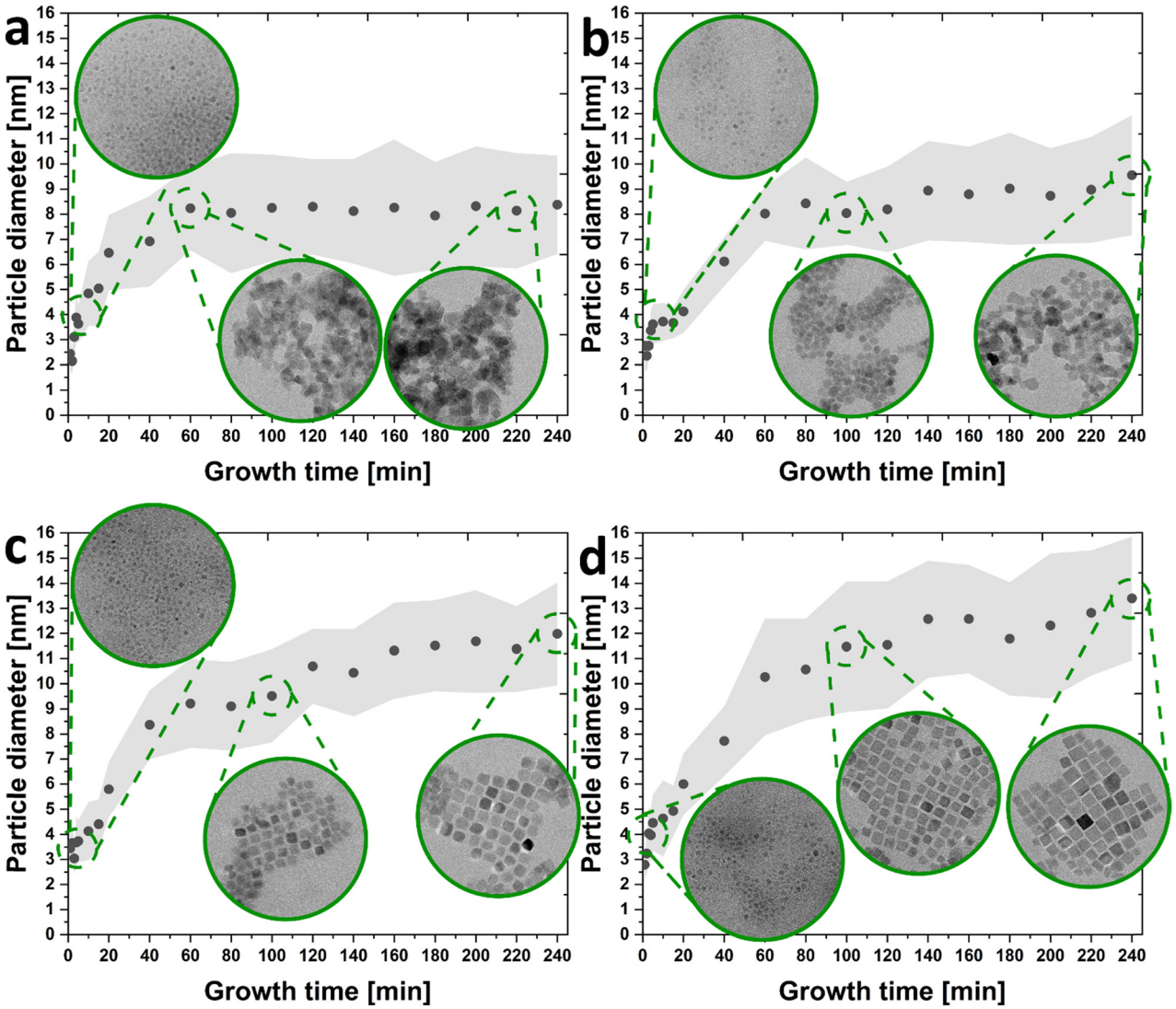

Fig. 2 Growth series of Co_3O_4 nanoparticles in an up-scaling approach with tripled reagent masses and reaction volume. Particle growth was monitored over a 4h period after the injection of NaOH. Growth curves are depicted for NPs prepared with a) $n(Co(NO_3)_2{\cdot}6H_2O)$ = 6 mmol (100^{4h}_{6mmol}), b) $n(Co(NO_3)_2{\cdot}6H_2O)$ = 12 mmol (100^{4h}_{12mmol}), c) $n(Co(NO_3)_2{\cdot}6H_2O)$ = 18 mmol (100^{4h}_{18mmol}), and d) $n(Co(NO_3)_2{\cdot}6H_2O)$ = 24 mmol (100^{4h}_{24mmol}) in 60 mL OLA. The insets show TEM micrographs of aliquots extracted at the indicated growth stages (green circles).

ensuring minimal influence on the results due to the loss in reaction volume. Particle growth was allowed to proceed for 4 h after NaOH injection with $n(Co(NO_3)_2{\cdot}6H_2O)$ set to 6, 12, 18, and 24 mmol, respectively. Accordingly, the sample types considered in the growth time-dependent evaluation are termed 100^{4h}_{6mmol}, 100^{4h}_{12mmol}, 100^{4h}_{18mmol}, and 100^{4h}_{24mmol}. A reaction temperature of T = 100 °C was chosen for the growth experiments in line with the narrowest received PSDs of the initially performed 1 h reactions displayed in Table 1. Since each aliquot represents a growth stage frozen in time and the specimens are prepared on a small copper grid for TEM analysis, minor data outliers are to be expected due to the mechanism of Ostwald ripening. Thus, there might be a slightly higher or lower fraction of larger particles (than the actual average) randomly found in individual samples.[20]

In the early minutes of the reaction progress, the particle count generally remains low, while the particle size increases relatively fast until t = 20 min. Slow growth during an onset period is not observable. Subsequently, the particle count steadily increases until *ca.* t = 60 min in all growth series. Conspicuously, however, the size increases more rapidly for higher concentrations (compare Fig. 2a *vs.* d). For sample 100^{4h}_{6mmol} prepared with the lowest reagent concentration, the size stabilizes around 8 nm past 60 min, indicating monomer pool depletion. The PSD begins to broaden at T = 80 min (*cf.* Table S4†). For this reason, we suggest terminating the synthesis after 60–80 min in this case. In the other three experiments operating at higher Co(II) concentrations, particle growth continues past 60 min with the smallest increase in size shown by sample 100^{4h}_{12mmol}. Although slow, but steady growth is observed even past 120 min, the PSD increases substantially (*cf.* Table S5†) and the experiment should therefore be terminated between 120–180 min for optimal results. Sample 100^{4h}_{18mmol} exhibits steady growth and may safely be terminated past 180 min to maximize particle yield (*cf.* Table S6†). Similar to sample 100^{4h}_{6mmol} (*cf.* Fig. 2), the morphology of the 100^{4h}_{18mmol} particles evolves from a cuboidal to a cubic shapes over time. The highest concentrated sample type 100^{4h}_{24mmol} provides the largest particles among the four considered growth experiments, displaying a well-developed cubic particle shape, while the PSD remains relatively narrow until t = 240 min, thus suggesting the experiment may be terminated between 180–240 min (*cf.* Table S7†). Notably, sample type 100^{4h}_{18mmol} produces the narrowest PSDs during 4 h of particle growth (*cf.* Table S8†). Although the observed PSD of 100^{4h}_{24mmol} is slightly broader, this reaction yields a larger size and a more pronounced, faceted cubic shape (*cf.* Fig. S12†). Hence, control over blunting of edges and corners can also be achieved by adjusting concentration and growth time, thereby potentially influencing the tendency for NP self-assembly and the geometry of the attainable superstructures.[21] It should be kept in mind, though, that mature, purified particles (extracted from a batch synthesis without aliquot extraction) may be slightly larger than comparable NPs in the aliquots (deviation *ca.* 1 nm) since in the final stages of conversion and purification the particles can grow further during the removal of co-solvents and heating to 180 °C. For 100^{4h}_{6mmol}, this effect is less pronounced considering that the monomer pool is depleted.

Overall the obtained growth curves (Fig. 2) align well with expected growth behaviour as compared to existing literature.[22–25] Based on classical nucleation theory, a slow and continuous increase in particle size leading into a plateau is caused by adsorption-controlled growth limited by the surface growth reaction.[26] However, the same observation may also be described by a (non-classical) two-step nucleation model,[27] which appears more applicable to our data.[28] A clear indicator in favour of this assumption is the rising particle count we observe throughout the experiment. As proposed by Finke and Watzky, NPs do not nucleate instantaneously but continuously as long as the required conditions for nucleation are fulfilled, in particular with respect to the supersaturation.[29–31] Fig. 3 schematically illustrates the proposed stages of the particle growth process based on the example of the 100^{4h}_{18mmol} growth curve (*cf.* Fig. 2c). The particles nucleate in a small, quasi-spherical shape and proceed to grow *via* a cuboidal morphology into their final clearly facetted cube-shaped appearance as evidenced by TEM micrographs (*cf.* insets in Fig. 2). This conspicuous morphological transition poses another indication for a non-classical crystallization mechanism where nucleation is described as the condensation of a dense (disordered) phase, which crystallizes during further growth.[32–34] Such an initially isotropic phase would adopt a spherical or quasi-spherical appearance to minimize its surface energy.[35–38] Therefore, we interpret the initial quasi-spherical shape of the particles in

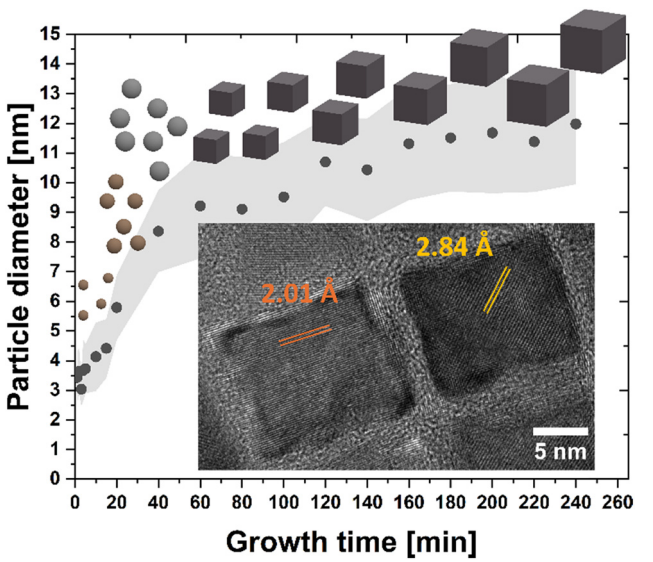

Fig. 3 Schematic illustration of particle growth stages on the background of the growth curve obtained for sample 100^{4h}_{18mmol} (black circles). Inset: HRTEM of crystalline Co_3O_4 nanocubes with lattice fringes exhibiting characteristic spacings of d = 2.01 Å and d = 2.84 Å corresponding to the {004} and {022} planes of Co_3O_4, respectively.

this work as a remnant of the nucleation process. With increasing size and crystallinity, the NPs then grow more and more into a cubic morphology, which represents the equilibrium shape of crystals with the Co_3O_4 spinel structure.[39,40] The crystalline character of the nanocubes throughout their entire volume is exemplarily shown in the HRTEM micrograph presented in Fig. 3 (inset) where characteristic lattice fringes attributable to Co_3O_4 may be observed. The extracted lattice distances of d = 2.01 Å and d = 2.84 Å can be assigned to the {004} and {022} lattice planes of the spinel structure (*cf.* Fig. S2 and S3†). Following a non-classical growth model, the particles undergo fast autocatalytic growth between 1–40 min of reaction time, followed by a reduction of the growth rate. Newly nucleated, smaller particles grow faster than larger ones due to a steeper concentration gradient between the bulk solution and the particle surroundings.[18,26,41] With a rising particle count, more monomer units are siphoned towards smaller particles which leads to an equilibration of the size in the NP ensemble. As a result, we are observing slow particle growth, approaching a plateau after t = 60 min, but no significant broadening of the PSD (depending on concentration and growth time). According to a model developed by Alexandrov and Makoveeva, two-step nucleation may involve a short diffusion-controlled growth regime prior to the adsorption-controlled growth.[27] We indeed observe a slightly steeper rise in particle size between t = 0–20 min (*cf.* Fig. 2), where the particles are growing fast to approximately half of the later total size. Based on the limited time resolution of the presented data, however, conclusive evidence on the mechanism at very early stages of growth cannot be deduced.

In view of systematically tailoring NP size and PSD depending on the chosen reaction conditions, the established growth curves can give important insights into particle sizes and PSDs to be expected during the preparation of NPs with the applied synthetic strategy for specific growth times.

Conclusions

In summary, colloidally stable Co_3O_4 NPs with sizes ranging from 5–16 nm have been successfully synthesized in ambient atmosphere (*cf.* Fig. 1 and 2). The presented synthetic approach allows for predictable adjustments of nanoparticle sizes and PSDs by systematic variations of the Co(II) salt concentration (0.1–0.4 M) and the reaction temperature (T = 60–100 °C; *cf.* Table 1). The particle morphology undergoes a prominent transition from cuboidal to cubic shapes for Co(II) salt concentrations of ≥0.3 M at T = 90 °C and T = 100 °C.

Narrow PSDs (as low as 12% for sample type 100^{1h}_{8mmol}) are achieved without the necessity for size-selective precipitation at reaction temperatures of T = 90 °C and T = 100 °C, where PSDs of ±15% or less have been previously described as narrow in the sense of near-monodispersed.[28] Based on the solubility limit, the maximum loading of the reaction with $Co(NO_3)_2{\cdot}6H_2O$ is estimated to be in the range between 8 mmol and 10 mmol (in 20 mL with 2 mL EtOH as phase mediator).

Most importantly, in view of practical applications, *e.g.* in heterogenous catalysis, the presented synthetic strategy is scalable, such that longer growth times along with up-scaling the reagent concentrations reliably increase the NP yield per experiment.

Based on the established growth curves obtained under systematic variation of reaction time and reagent concentrations, we can deduce optimal termination times for the individual experiments (100^{4h}_{6mmol} (t = 60–80 min), 100^{4h}_{12mmol} (t = 120–180 min), 100^{4h}_{18mmol} (t = 180–240 min), and 100^{4h}_{24mmol} (t = 180–240 min)) to achieve the most favourable results. For samples 100^{4h}_{18mmol} and 100^{4h}_{24mmol} narrow PSDs may still be achieved for growth times >180 min.

As the NP morphology and the degree of edge blunting can also be controlled *via* the reaction parameters, the presented synthetic strategy opens interesting perspectives for NP self-assembly into colloidal crystals with tuneable packing structures and potential emerging properties based on cooperative effects between the particles.

Data availability

Data for this article, including transmission electron micrographs (TEM) and powder X-ray diffraction (PXRD) files are shown in the ESI† and will be archived and made available *via* the RADAR platform at **https://www.radar-service.eu/radar/en/home** upon publication or on request.

Conflicts of interest

There are no conflicts to declare.

Acknowledgements

This work was supported by the Deutsche Forschungsgemeinschaft (DFG, German Research Foundation) *via* Collaborative Research Centres CRC 840 (subproject B09) and CRC 1585 (Project No. 492723217, subproject A03). We acknowledge the Bavarian Polymer Institute (BPI) for providing access to electron microscopy facilities within the Keylab "Electron and Optical Microscopy". The authors are grateful to Sabine Rosenfeldt as well as Benedikt Wirth (University of Bayreuth) for the acquisition of X-ray diffraction data and assistance in nanoparticle synthesis, respectively.

Notes and references

1 Y. Yin and A. P. Alivisatos, *Nature*, 2005, **437**, 664–670.
2 Y. Ding, C. Wang, M. Zeng and L. Fu, *Adv. Mater.*, 2023, 2306689.
3 A. L. Efros and L. E. Brus, *ACS Nano*, 2021, **15**, 6192–6210.
4 M. V. Kovalenko, L. Manna, A. Cabot, Z. Hens, D. V. Talapin, C. R. Kagan, X. V. I. Klimov, A. L. Rogach, P. Reiss, D. J. Milliron, P. Guyot-sionnnest, G. Konstantatos, W. J. Parak, T. Hyeon, B. a. Korgel, C. B. Murray and W. Heiss, *ACS Nano*, 2015, **9**, 1012–1057.

5 C. Xie, Z. Niu, D. Kim, M. Li and P. Yang, *Chem. Rev.*, 2020, **120**, 1184–1249.
6 J. B. Gerken, J. G. McAlpin, J. Y. C. Chen, M. L. Rigsby, W. H. Casey, R. D. Britt and S. S. Stahl, *J. Am. Chem. Soc.*, 2011, **133**, 14431–14442.
7 C. Lu, L. Liu, Y. Yang, Y. Ma, Q. Luo and M. Zhu, *ChemNanoMat*, 2023, **9**(5), e202200537.
8 N. Goel, K. Kunal, A. Kushwaha and M. Kumar, *Eng Rep.*, 2023, **5**, 1–22.
9 A. J. Esswein, M. J. McMurdo, P. N. Ross, A. T. Bell and T. D. Tilley, *J. Phys. Chem. C*, 2009, **113**, 15068–15072.
10 L. Nie, Z. Li, T. Kuang, S. Lyu, S. Liu, Y. Zhang, B. Peng, J. Li and L. Wang, *Chem. Commun.*, 2019, **55**, 10559–10562.
11 N. E. Tsakoumis, E. Patanou, S. Lögdberg, R. E. Johnsen, R. Myrstad, W. van Beek, E. Rytter and E. A. Blekkan, *ACS Catal.*, 2019, **9**, 511–520.
12 X. Deng and H. Tüysüz, *ACS Catal.*, 2014, **4**, 3701–3714.
13 Y. Song, B. Xu, T. Liao, J. Guo, Y. Wu and Z. Sun, *Small*, 2021, **17**, 1–21.
14 T. Reier, H. N. Nong, D. Teschner, R. Schlögl and P. Strasser, *Adv. Energy Mater.*, 2017, **7**(1), 1601275.
15 J. Kießling, S. Rosenfeldt and A. S. Schenk, *Nanoscale Adv.*, 2023, **5**, 3942–3954.
16 S. G. Kwon and T. Hyeon, *Acc. Chem. Res.*, 2008, **41**, 1696–1709.
17 S. G. Kwon and T. Hyeon, *Small*, 2011, **7**, 2685–2702.
18 T. Sugimoto, *Adv. Colloid Interface Sci.*, 1987, **28**, 65–108.
19 D. R. Lide and G. Baysinger, *CRC Handbook of Chemistry and Physics*, CRC Press, 90th edn., 2010.
20 C. L. Kuo and K. C. Hwang, *Chem. Mater.*, 2013, **25**, 365–371.
21 J. S. N. Brunner, B. Maier, S. L. J. Thoma, F. Kirner, I. A. Baburin, D. Lapkin, R. Rosenberg, S. Sturm, D. Assalauova, J. Carnis, Y. Y. Kim, Z. Ren, F. Westermeier, S. Theiss, H. Borrmann, S. Polarz, A. Eychmuller, A. Lubk, I. A. Vartanyants, H. Colfen, M. Zobel and E. V. Sturm, *Chem. Mater.*, 2021, **33**, 9119–9130.
22 K. Ahrenstorf, H. Heller, A. Kornowski, J. A. C. Broekaert and H. Weller, *Adv. Funct. Mater.*, 2008, **18**, 3850–3856.
23 K. M. Ø. Jensen, M. Christensen, P. Juhas, C. Tyrsted, E. D. Bøjesen, N. Lock, S. J. L. Billinge and B. B. Iversen, *J. Am. Chem. Soc.*, 2012, **134**, 6785–6792.
24 F. Yang, *Langmuir*, 2021, **37**, 3912–3921.
25 A. N. Solodov, J. R. Shayimova, E. A. Burilova, D. V. Shurtakova, Y. I. Zhuravleva, M. A. Cherosov, Y. Tian, A. G. Kiiamov and R. R. Amirov, *J. Phys. Chem. C*, 2021, **125**, 20980–20992.
26 T. Wen, X. Zhang, D. Zhang, C. Zhang, Q. Wen, H. Zhang and Z. Zhong, *J. Phys. Chem. C*, 2018, **122**, 27070–27081.
27 D. V. Alexandrov and E. V. Makoveeva, *J. Appl. Phys.*, 2023, **134**(23), 234701.
28 M. A. Watzky and R. G. Finke, *J. Am. Chem. Soc.*, 1997, **119**, 10382–10400.
29 T. Sugimoto, *J. Colloid Interface Sci.*, 2007, **309**, 106–118.
30 J. D. Martin, *Chem. Mater.*, 2020, **32**, 3651–3656.
31 R. G. Finke, M. A. Watzky and C. B. Whitehead, *Chem. Mater.*, 2020, **32**, 3657–3672.
32 R. P. Sear, *J. Chem. Phys.*, 2009, **131**(7), 074702.
33 M. A. Boles, M. Engel and D. V. Talapin, *Chem. Rev.*, 2016, **116**, 11220–11289.
34 S. Özkar and R. G. Finke, *J. Am. Chem. Soc.*, 2017, **139**, 5444–5457.
35 W. Ostwald, *Z. Phys. Chem.*, 1897, **22U**(1), 289–330.
36 M. Volmer and A. Weber, *Z. Phys. Chem.*, 1926, **119U**, 457.
37 W. Thomson, *Lond. Edinb. Dubl. Phil. Mag.*, 1871, **42**, 448–452.
38 P. Rein ten Wolde and D. Frenkel, *Phys. Chem. Chem. Phys.*, 1999, **1**, 2191–2196.
39 L. Liu, Z. Jiang, L. Fang, H. Xu, H. Zhang, X. Gu and Y. Wang, *ACS Appl. Mater. Interfaces*, 2017, **9**, 27736–27744.
40 J. M. Rahm and P. Erhart, *Nano Lett.*, 2017, **17**, 5775–5781.
41 H. Reiss and V. K. La Mer, *J. Chem. Phys.*, 1950, **18**, 1–12.

